Experimental and theoretical investigations on high-ash coal-air flames in high-speed jets stabilized recirculating flow

Mani Kalyani Ambatipudi*[1] and Varunkumar S[1]

[1] *Department of Mechanical Engineering, IIT Madras, Chennai, India*

Abstract

In this paper, experimental and theoretical investigations on the stability of coal-air flames in high-speed jets stabilized recirculating flow are presented. The current work reports the operational limits of high-ash coal-air flames stabilized by large velocity differentials. Experiments are performed to investigate the effects of particle size distribution, flow rate of primary and high-speed jets, and feed rate of coal on the stability of recirculating coal-air flames. Temperature measurements of the primary reaction zone are used to assess the stability of the reactor under various operating conditions. Experiments are carried out with two different particle size distributions, namely: (1) the fine (< 355 μm), and (2) the coarse (< 700 μm) distributions. Investigations are carried out with a range of primary jet velocities (4 m/s to 9 m/s), high-speed jets mass flow rates (1.24×10^{-3} to 4.94×10^{-3} kg/s) and feed rates (1.11×10^{-3} to 2.1×10^{-3} kg/s). A non-dimensional *ignition index* (τ) which is a ratio of the particle flow time (t_f) to particle ignition time (t_{ig}) is shown to indicate the stability of recirculating coal-air flames. Temperature measurements indicate that the operating conditions with $\tau > 0.6$ are stable whereas those with $\tau < 0.6$ lead to reactor quenching. Force balance on particles with numerically resolved velocity profiles is used to estimate the particle flow time. Particle ignition times are quantified by the extended *unified ignition-devolatilization model*. Results indicate a strong influence of primary jet velocity on the stability of the flame. Only a marginal increase in stability can be attributed to the high-speed jets. Particle size distribution, along with the feed rate plays a crucial role in determining

*manikalyani24@gmail.com

the stability of recirculating coal-air flames. Temperatures with the fine distribution exceed ash fusion temperature causing slag deposition in the reactor. Model-based inferences on the increase in stability of recirculating coal-air flames with preheated coal are presented.

Keywords: recirculating coal-air flames; ash-fusion; stability regimes; high-ash coal; zero preheating

1 Introduction

Utilization of high-ash coals in thermo-chemical conversion processes in general and gasification in particular, is restricted by the ash fusion limits. This issue has been a major constraint in the development of large scale thermo-chemical conversion systems with high-ash Indian coals for combined cycle power generation and process applications.

Significant number of commercial gasifiers using high-rank coals are of slagging type. These gasifiers typically use low to moderate ash coals (<25%). However, utilizing high-ash low-rank coals in a slagging type gasifier is not advantageous for the following reasons: (i) high ash coal would lead to a low cold gas efficiency as a significant fraction of energy is required for melting a large amount of ash. (ii) the recommended value of slag viscosity for efficient trapping of slag is < 25 Pa-s over the preferred temperature range of 1300–1500°C (Harris and Patterson, 1995; Kong et al., 2014; Lowry, 1963; Mishra et al., 2020; Patterson and Hurst, 2000; Wang and Massoudi, 2013). However, the high-ash Indian coals have a slag viscosity 298-40 Pa-s in the temperature range of 1300–1500 °C (Mishra et al., 2020), and are low to moderate slagging (Sharma et al., 2014). The addition of large amounts of flux, given the low calorific value of low-rank coals, is also uneconomical. This makes Indian coals incompatible for slagging gasifiers. Therefore, for the utilization of high-ash low-rank Indian coals, designs of gasifiers that prevent ash-fusion are essential. To avoid ash fusion, reactor configurations with precise control over oxygen concentration and temperature distribution are necessary.

Moderate or Intense Low oxygen Dilution (MILD) combustion offers the flexibility of control over temperature distribution and oxygen concentration profiles besides providing enhanced thermal efficiency and a simultaneous reduction in pollutant emissions (Cavaliere and de Joannon (2004)). MILD

combustion of solid fuels is an emerging area of research and the current work is motived by the need for a MILD like solid fuel thermo-chemical conversion system for gasification and combustion applications. In the case of solid fuels with high ash, creating MILD like conditions offer not just clean combustion but also is a necessity from ash fusion perspective, and its detrimental effect on carbon conversion and hence combustion efficiency. MILD combustion of coal has received considerable attention in the recent past for its advantages in reducing NO_x emissions. The focus of all these earlier works was on measuring and estimating NO_x emissions in overall fuel-lean environments (ϕ <1). However, MILD coal combustion in the context of suppression of ash fusion has received very little attention in the literature. Low and uniform temperatures in MILD combustion can be capitalized to prevent slag formation and associated poor carbon conversion.

The aim of the current study is to identify the operational limits of high-ash coal-air flames in recirculating flows induced by high-speed jets. Two limits of desirable operating conditions of such reactors are imposed by temperatures either exceeding the ash-fusion temperatures or leading to quenching of the reactor. The current study is aimed at identifying the effects of various parameters that lead to a stable volatile oxidation zone, not exceeding the ash-fusion temperature in fuel-rich conditions that are relevant for gasification.

1.1 Earlier studies

Earlier efforts on MILD coal combustion were mostly focused on investigations on NO_x emissions. Many of these studies can be classified as simulated MILD processes, wherein, the enthalpy addition by coal is much lower than external enthalpy addition (Saha et al. (2016, 2017)), or coal injection in vitiated combustion products of gaseous fuels (Weber et al. (2005)), or by maintaining the wall temperatures of the reactor in the range of 900-1300°C with external electric heating (Ristic et al. (2008); Stadler et al. (2011, 2009)). Though the information from these studies cannot be extrapolated to self-sustained combustion processes, the data can be used to validate sub-models for coal operating under MILD conditions.

Weidmann and co-workers (Weidmann et al. (2016, 2015)) presented detailed measurements on MILD coal combustion characteristics of low ash coals operating close to stoichiometric conditions ($\phi \sim 1$ – 1.13). Li et al.

(2014) established MILD combustion with two different burners using coal with ∼30% ash. Zhang et al. (2007) investigated MILD coal combustion and NO_x emission characteristics of pulverized coal in a primary air enrichment and preheating (PRP) burner. Zhang et al. (2017), continuing the work reported in Zhang et al. (2007), used O_2 enriched air for ignition improvement and flame stability. Stable operating conditions shown in all these studies can be attributed to the particle size effects. Pulverized particles have shorter thermal response time compared to the size distributions used in the current work. Moreover, the emphasis of all these studies was to correlate emission characteristics to the temperature profiles in the reactor in fuel-lean operating conditions. The results obtained from these studies are not directly relevant to gasification regimes operating under fuel-rich conditions.

Fu et al. (1988) were the first to employ off-axis asymmetric co-flowing jets with large velocity differentials (20 m/s primary velocity, high-speed jets were injected near sonic speed) to stabilize low grade pulverized coal flames without preheated air. Aerodynamics of the jets control and maintain the recirculation, temperature and species profiles in this configuration. Though, they attributed the increased stability of the reactor to the aerodynamic action of the primary and high-speed jets, the effect of jet velocities on the stability of the reactor was not brought out. Fundamental features governing the stability of the reactor were not investigated in detail. This configuration has been adopted in the current study for its simplicity in controlling the temperature profiles. A detailed description and scaling criteria of the reactor are presented later.

A few earlier works explored the fundamental aspects of MILD coal combustion and the parameters that affect the burning characteristics of coal. Mao et al. (2017) experimentally investigated MILD combustion of low ash coal with primary air heated to 100°C and high-speed jets heated to 200°C. Suda et al. (2002) experimentally investigated the effects of air temperature on ignition of coal in recirculating coal-air flames. Both the works qualitatively presented that the coal-air flames were stable at high air preheating, and Suda et al. (2002) reported a dramatic increase in stability with an increase in air temperature. Mei et al. (2013) numerically studied the effects of primary and high-speed jet velocities on the MILD combustion characteristics of coal. They reported that varying primary jet velocity has

more influence on the temperature profile than the secondary jet, a result that is consistent with the current work. Their results indicate an increase in ignition delay as the primary jet velocity is increased. They also reported that increasing the primary jet velocity to 99 m/s, destroys fuel-rich and fuel-lean zones, causing a merger of the primary and secondary flames. However, no such observation can be made from the current work and temperature and volatile realease contours reported by Saha et al. (2016).

Saha et al. (2017) experimentally studied the impact of particle size on the combustion characteristics of coal with two particle size distributions, namely, 53–125 μm and 250–355 μm, in a simulated MILD environment. The differences in the onset of devolatilization were attributed to particle dispersion in the jet and Stokes number variation. Volatile release contours indicate the onset of devolatilization for 53–125 μm case even before any dispersion. Therefore, the observed differences are likely due to longer ignition time for larger particles compared to smaller particles. Saha et al. (2014) numerically investigated the effects of coal particle diameter in a self-recuperative furnace. They reported a negligible impact of particle size on achieving MILD conditions, which in the light of the effect of particle size brought out above, seems incorrect. Temperature contours presented depict the differences due to the two particle sizes. With the large particle (180 μm), the centerline temperatures are lower, indicating that the ignition is delayed compared to the smaller particle (38 μm) case.

Summarizing, the emphasis of the earlier literature on MILD coal combustion was to investigate the NO_x formation and destruction mechanisms. All the studies were restricted to pulverized sized class coal and fuel-lean ($0.8< \phi \leq 1$) operating conditions excepting the work of Stadler et al. (2011). No studies on recirculating coal-air flames operating under fuel-rich conditions can be found in the literature, at least to the best of the authors knowledge. Fundamental studies on the effects of various operating parameters on MILD coal combustion characteristics are seen to have contradicting results, indicating a need for further investigation.

The current study aims to identify stable operating conditions under fuel-rich conditions (aimed at gasification applications) in a self-sustained process with temperatures not exceeding the ash-fusion temperature. The impact of airflow distribution between primary and high-speed jets, particle size distribution and feed rate on the stability of fuel-rich coal-air flames is

addressed in the current work. A non-dimensional number is proposed to unify the observed behaviour with a theoretical framework. The theoretical framework is used to infer the impact of coal preheating on the stability of recirculating coal-air flames. The rest of the paper is organized in the following manner: (1) experiments, (2) results, (3) particle sub-models, (4) stability analysis, and (5) conclusions.

2 Experiments

2.1 Reactor Design

The reactor design used in the current study is based on the configuration studied by Fu et al. (1988). Flux based scaling procedure is adopted to scale down the 1.3 MWth reactor used in Fu et al. (1988) to a 50 kWth burner for the current work. Flux-based scaling has the advantage of preserving the flow structure Edland et al. (2019); Smart and Morgan (1994); Weber and Breussin (1998) and particle scaled time-temperature history. The procedure for scaling down the reactor is given below.

Coal feed rate was determined initially for scaling down the reactor to 50 kWth capacity. The primary flow rate was determined by maintaining the coal to primary mass flow rate identical as in Fu et al. (1988). The primary diameter was calculated by equating the primary air flux for 1.3 MWth reactor and 50 kWth reactors, preserving the primary jet velocity. High-speed jets (HS jets) flow rate was obtained by fixing the ratio of high-speed jet to primary jet airflow rate constant as in Fu et al. (1988). Maintaining the high-speed jets flux equal for 1.3 MWth and 50 kWth, yielded the high-speed jets diameter to be about 1.3 mm. To explore the effect of this parameter experiments were conducted with 1 mm and 2 mm high-speed jets diameter. Geometric similarities were maintained by fixing the ratio of the reactor diameter to primary diameter identical. Table 1 presents an overview of the scaling procedure, design values and realized values.

Table 1: Scaling procedure for the current reactor design.

Parameter	**Parameters used in Fu et al. (1988)**	**Design parameters (realized values)**
Power (MW)	1.31	0.05 (0.04-0.02)
Coal feed rate (kg/s)	0.056	0.0028 (0.0021-0.0011)
Coal/Primary air flow rate	0.233	0.233 (1.38-0.3)
Primary air flow rate (kg/s)	0.24	0.012 (0.0015-0.0035)
Primary jet flux (kg/m^{2}s)	31.7	31.7 (4.77-11.62)
Primary jet diameter (mm)	98	22 (20)
Primary jet velocity (m/s)	25.6	25.6 (4-9)
High-speed jets/Primary jet air flow rate	0.0712	0.0712 (3.3-0.34)
High-speed jet flux (kg/m^{2}s)	307.52	307.52 (1466-1528)
High-speed jet flow rate (kg/s)	0.0167	0.0008 (0.0012-0.005)
High-speed jet diameter (mm)	8.3	1.3 (1 & 2)
High-speed jet velocity (m/s)	248	248 (supersonic)
Reactor/Primary diameter	4.3	4.3 (4.3)
Reactor ID (mm)	420	94 (108)

While the coal feed rate and reactor dimensions were realized as per the results of the scaling procedure, the primary jet and high-speed jets flow rates differed considerably from the design values. This is due to the differences in particle size distribution used in the current work and that used in Fu et al. (1988). When attempts were made to use the same velocities as that in Fu et al. (1988) with coarse particle size distributions, it was found to result in a highly unstable primary reaction zone. As the coarse fraction increased, the coal-air flame stabilized away from the burner when the primary jet velocity exceeded 6 m/s (to be discussed later). To compensate for this effect, primary flow rate is brought down to ensure the coal-air flame is stabilized close to the burner with a simultaneous increase in the high-speed jet flow rate to account for the reduction in air-fuel ratio.

Experiments were performed in a recirculating reactor adopting the scaling procedure discussed above, a schematic of which is presented in Fig. 1. The reactor consists of a burner, a combustion chamber, a cyclone separator, and a convergent section connecting the combustion chamber to the cyclone separator; all made of SS 316. A recirculation zone in the reactor was formed by the velocity differences of the primary and high-speed jets.

The burner had a central primary jet, and two pairs of holes of diameters 1 mm and 2 mm drilled off-axis into the burner, which acted as a source of high-speed jets as shown in Fig. 2. Either 1 mm holes or 2 mm holes were used in any given experiment. The combustion chamber was a cylinder of 108 mm diameter and 720 mm in length. The combustion chamber was attached to the burner on one end and a cyclone separator on the other end through a converging section of 300 mm. The reactor was equipped with provisions for 5 temperature measurements along the length of the reactor. Coal was fed into the reactor by an electromagnetic vibratory feeder into a funnel present on the primary line. An orifice present upstream of the funnel entrained coal into the primary jet. Air was also entrained into the primary jet from the ambient through this arrangement. Table 2 shows the entrained airflow rate variation with the primary jet flow rate. The reactor was also furnished with two view-ports, one at 30 mm from the burner head, other at 30 mm before the converging section for visual examination of the flame. Properties of coal pertinent to the current discussion are presented in Table 3.

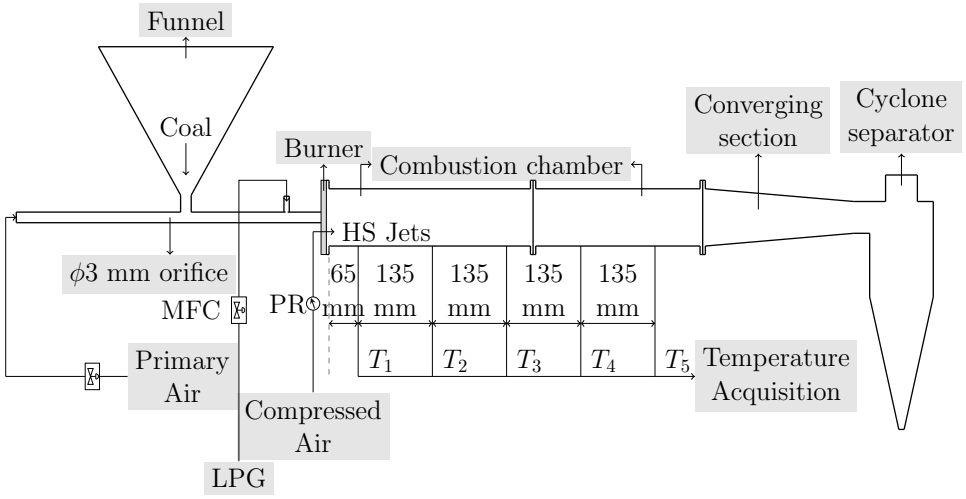

Figure 1: Schematic of the experimental setup.

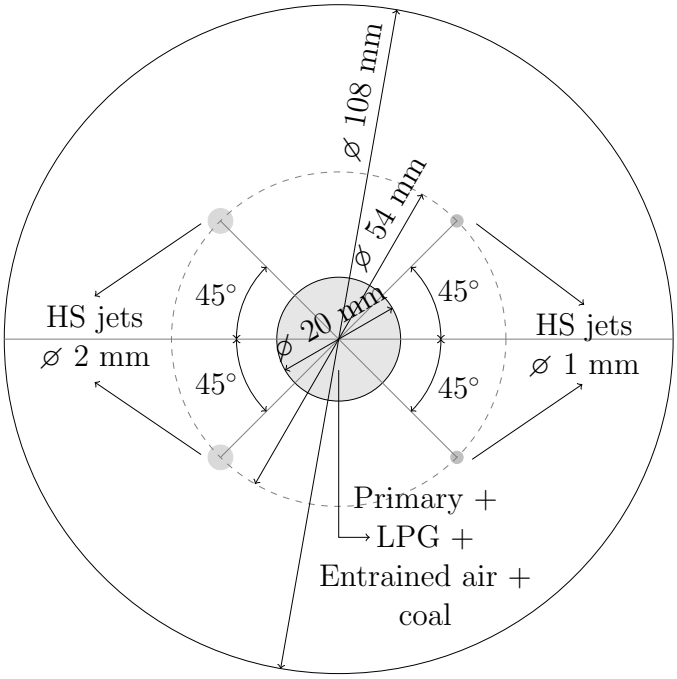

Figure 2: Burner geometry.

Table 2: Entrained air flow rate vs primary air flow rate.

Primary jet air flow rate $\times 10^{-3}$ (kg/s)	**Entrained air flow rate** $\times 10^{-3}$ (kg/s)	**Total primary airflow rate** $\times 10^{-3}$ (kg/s)	**Velocity of the primary jet** (m/s)
0.60	0.88	1.48	4
1.00	1.38	2.38	6.3
1.40	2.01	3.41	9

Table 3: Properties of coal used in the current study - proximate and ultimate analysis.

Property	**Value**
Density (kg/m^3)	1400
Proximate analysis	
Volatile fraction[*], %	42.5
Char content[*], %	42.5
Moisture fraction[*], %	15
Ash content, %	30-40
Ultimate Analysis[**]	
C %	66
H %	6
O %	24
N %	4
$(A/F)_{stoichiometric}$[***]	5.09
LCV (MJ/kg)[*]	24
Ash fusion temperature (°C)	1200

[*] - ash-free basis
[**] - dry ash-free basis
[***] - as received basis

2.2 Experimental Methodology

The objective of the current study is to delineate the regimes of stability and operational limits of high-ash coal-air flames in high-speed jets stabilized reactor. Temperature measurements were used to determine the stability of the flame. Temperatures were measured by 5 R-type thermocouples (1 mm diameter) placed at regular intervals of 135 mm along the length of the reactor. The first thermocouple was placed 65 mm from the burner head (refer Fig. 1). Temperature data was logged by a data logger at a frequency of 1 Hz. Flow rates of the primary and LPG jets (used for ignition) were controlled by mass flow controllers (MFC) of 500 lpm and 50 lpm respectively (accuracy of 1% of full scale). The high-speed jets flow rate was estimated from the pre-calibration of upstream pressure against airflow rate using an MFC.

Particle size distribution and feed rate of coal were set to required values by preprocessing coal before the start of each experiment. Preprocessing of coal included crushing, sieving coal to the desired particle size ranges, and calibrating the vibratory feeder. The particle size distribution (PSD) of a sample of prepared coal was determined by sieving and measuring the mass

present over a sieve by a 3 kg weighing balance before the start of each experiment. Two PSDs used in the current study are presented in Fig. 3. The coarse PSD had particles <700 μm and the fine PSD had sizes <355 μm. The spread in data for any given size class for both the PSDs was less than $\pm$10%. The feed rate of coal from the electromagnetic vibratory feeder was calibrated against voltage for each PSD. Feed rate during the experiment was set to required value based on the voltage and is cross-checked by coal feed rate measured during the experiment.

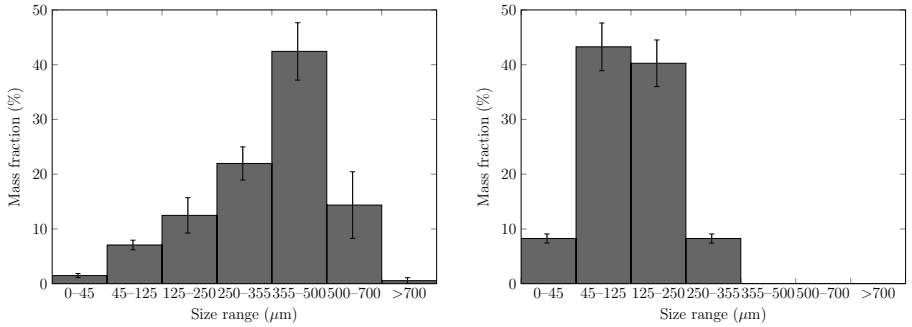

(a) The coarse PSD. (b) The fine PSD.

Figure 3: Particle size distributions used in the current work.

Experiments were started by heating up the reactor with LPG to about 1000°C and later switching to coal. An LPG flame was established by issuing 5 lpm LPG from the LPG inlet and 50 lpm air through the primary jet into the reactor. A lifted LPG flame was observed from the first view-port with the primary jet alone turned on. The high-speed jets were turned on after the second thermocouple (T_2) reached about 900°C. The pressure of the high-speed jets was progressively increased to 5 barG for 1 mm holes or 1 barG for 2 mm holes. Discharge of air from high-speed jets changed the operation of the LPG flame from a lifted flame mode to MILD like mode. Visual observations of the reactor transition to MILD mode through the view-port show a disappearance of jet flames into flameless combustion mode with uniform glow throughout the reactor. Uniformity of temperature measurements along the reactor length also suggests that the operation of the reactor is in MILD like mode. LPG flameless combustion was continued until all the thermocouple readings reached a steady value of about 1000°C. At this point, coal loading was started. Coal was weighed by a 3 kg weighing

balance (0.5 g accuracy) before loading to cross-check the obtained feed rate with the calibrated value. Loading was gradually increased until smoke was visible from the cyclone separator, indicating a transition to fuel-rich conditions. The LPG flow rate was progressively reduced to correspond to an increase in the coal feed rate. When the coal feed rate was set to the desired value, LPG was completely shut off. The primary flow rate and the pressure of the high-speed jets were fixed at this point. The time corresponding to these changes was noted. The experiment continued until the temperatures of all thermocouples attained steady-state before switching to the next set of conditions. The operating conditions were changed, and time was noted before the collection of data for a different experimental condition.

The stability regimes in the current work are reported as function of a non-dimensional ignition index, τ (details later). All the parameters of relevance are absorbed into τ. The uncertainties of various parameters are determined to calculate the uncertainty in τ. The uncertainty in the measurement of entrained air flow rate is around 15%. The thermocouples in the current work are calibrated and are certified to be accurate up to $\pm$ 2°C by the manufacturer. The feed rate from the vibratory feeder is accurate up to $\pm$ 11%. Accounting for errors in the estimation of particle flow time and particle ignition time, the uncertainty in the computation of τ is $\pm$ 12%.

3 Experimental results

3.1 The primary reaction zone

The first 200 mm of the reactor is considered as the primary reaction zone (PRZ). Since the focus of the current work is on stabilizing a coal-air flame with no preheating, this choice is considered reasonable. Also, results show that if the flame is not stabilized in the first 200 mm, the only downstream location which is favorable for stabilization is in the cyclone separator. Therefore, an operating condition is designated as a stable operating condition if the temperatures of the PRZ comprising thermocouples T_1 and T_2 were maintained above 900°C for at least 250 s.

If the PRZ is quenched, particles no longer travel through a favourable temperature field and hence the heat-up zone shifts downstream of the PRZ where temperatures are favourable for devolatilization and ignition. Due to this, the ignition and devolatilization zones are moved to the farther end of

the reactor. The shift of the heat-up zone continues due to the unfavourable temperature field, and subsequently, the entire reactor is cooled. Thus, the stability of the PRZ is an indicator of the stability of the entire reactor.

3.2 Regimes of reactor operation

Experiments in the current work can be classified into 4 categories based on the state of reactor operation as (1) stable without ash-fusion, (2) stable with ash-fusion, (3) quenched and, (4) chugging, characterized by periodic explosions. Experiments were conducted for a range of primary and high-speed jet flow rates, coal feed rate and particle size distributions. Associated nomenclature and the states of operation (stable/stable ash-fusion/quenched/chugging) are summarized in Table 4.

Table 4: Experimental operating conditions and nomenclature used in the current study.

Expt. name	Primary jet velocity (m/s)	High-speed jet mass flow rate $\times 10^{-3}$ (kg/s)	High-speed jet dia (mm)	Coal Feed rate $\times 10^{-3}$ (kg/s)	PSD	Remarks
Effect of primary flow rate						
P1	4	3.13	2	2.08	coarse	stable-no ash fusion
P2	6.3	3.13	2	2.08	coarse	stable-no ash fusion
P3	9	3.13	2	2.08	coarse	quenched
Effect of particle size distribution						
S1	4	2.63	2	2.08	coarse	stable-no ash fusion
S2	4	2.63	2	2.08	fine	stable-ash fusion
Effect of feed rate						
F1	4	2.21	1	2.08	coarse	stable-no ash fusion
F2	4	2.21	1	1.39	coarse	quenched
F3	4	2.63	2	1.67	fine	stable-ash fusion
F4	4	2.63	2	1.25	fine	stable-ash fusion
F5	4	2.63	2	1.11	fine	stable-ash fusion
Effect of high-speed jet flow rate						
H1	6.3	2.21	1	2.08	coarse	stable-no ash fusion
H2	6.3	1.91	1	2.08	coarse	stable-no ash fusion
H3	6.3	1.53	1	2.08	coarse	stable-no ash fusion
H4	6.3	1.24	1	2.08	coarse	stable-no ash fusion
H5	4	2.85	1	2.08	coarse	stable-no ash fusion
H6	4	3.25	1	2.08	coarse	stable-no ash fusion
H7	4	4.01	2	2.08	coarse	stable-no ash fusion
H8	4	4.94	2	2.08	coarse	stable-no ash fusion
H9	4	1.53	1	2.08	coarse	chugging

The reactor is termed stable without ash-fusion if the PRZ is maintained

between 900°C and 1200°C (ash-fusion temperature of coal used in the current work). The PRZ, in this case, supports the downstream endothermic processes and maintains the entire reactor at temperatures >900°C (refer Fig. 4a). Though the reactor is stable with temperatures exceeding 1200°C, it causes ash fusion as can be seen in Fig. 4b. It can be observed that for stable cases the temperature is more or less uniform at all axial locations (within ±125°C), indicating MILD like conditions in the reactor. Figure 5 shows an image of slag deposition observed in the reactor when the temperature in the PRZ exceeded 1200°C. For quenched conditions, as shown in Fig. 4c, the temperature in the PRZ is lower than 900°C. Heating of particles downstream cannot be sustained by the temperature profile in the PRZ, and results in subsequent quenching of the reactor as stated earlier.

With the coarse PSD and overall ϕ >3.5, volatiles released beyond z=0.6 m causes the coal-air flame to probably flashback until the coal funnel, causing a disruption in the coal feed rate. Disruptions in coal feed rate result in coupling of the coal feed rate and heat release rate, and results in a fluctuating temperature profile in the PRZ. The mean of the PRZ temperatures reduces due to the coupling, eventually leading to reactor quenching. (see Fig. 4d). Attempts were made to revive the reactor from quenching at about 400 s from the start of operation of H9 conditions (refer Fig. 4d). However, it was difficult to maintain the reactor under stable conditions after the reactor went into the chugging mode, in spite of the attempts made to stabilize the reactor.

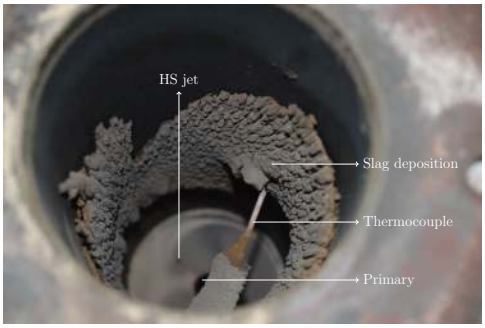

Figure 5: Slag deposition in the reactor observed with fine particle size distribution.

The effects of different operating conditions on the temperature profile in the PRZ are presented in Figs. 6 to 8 and are discussed in the following

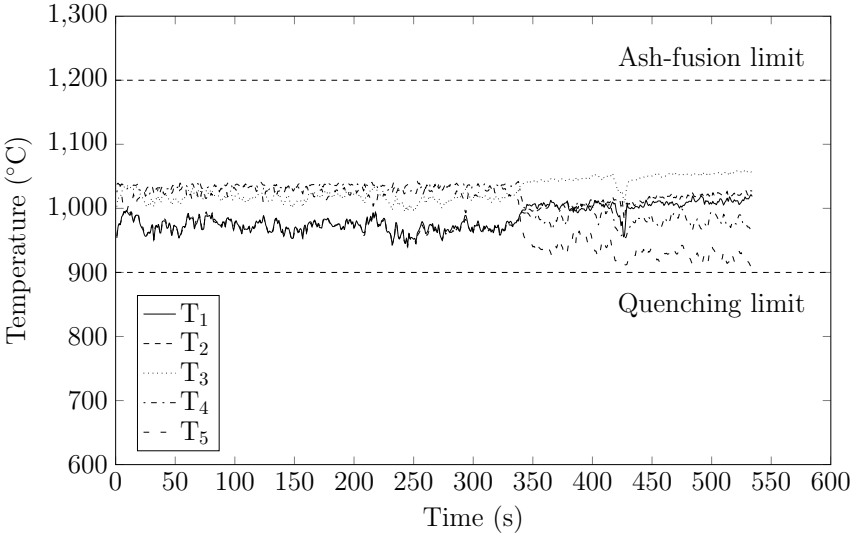

(a) P1 : stable and no ash-fusion.

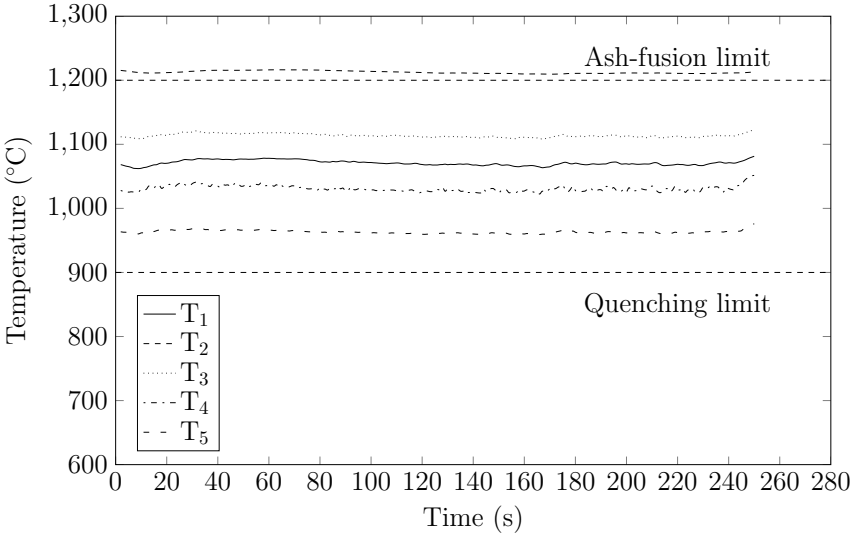

(b) S2 : stable and ash-fusion.

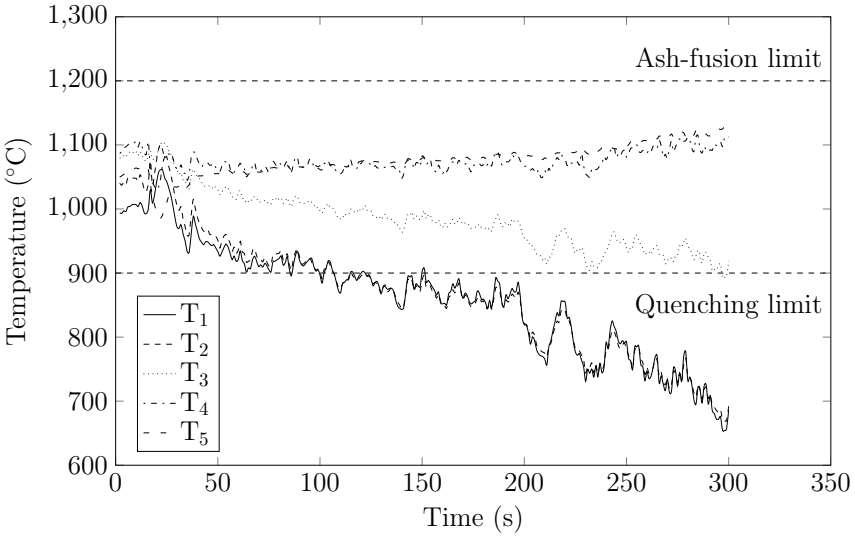

(c) P3 : quenched.

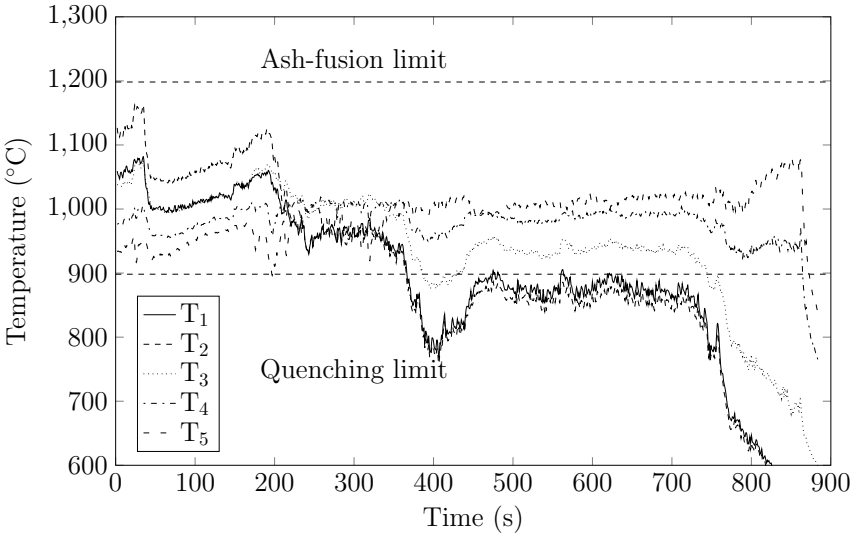

(d) H9 : chugging.

Figure 4: Different states of the reactor based on the operating conditions.

sections.

3.3 Effect of the primary jet flow rate

Figure 6 shows the effect of primary jet velocity on the temperature profiles and stability of the reactor at a given feed rate and coarse PSD. Experiments were performed with 3 different primary jet velocities. Operating conditions with primary jet velocities of 4 m/s and 6.3 m/s can be termed as stable-no ash fusion cases (P1, H5-H8, P2, H1-H4). Increasing the primary jet velocity beyond 6.3 m/s leads to reactor quenching (P3). As discussed earlier, increasing the primary jet velocity shifts the devolatilization zone downstream, leading to reactor quenching subsequently.

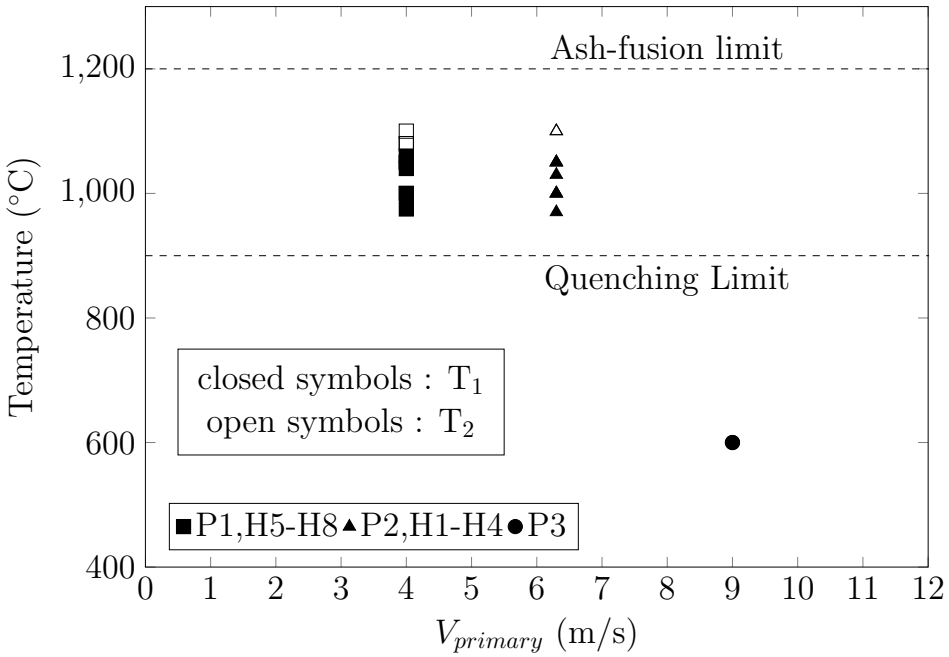

Figure 6: Effect of primary jet velocity on the PRZ temperature.

3.4 Effect of high-speed jets flow rate

Figure 7 shows the effect of high-speed jets flow rate on the temperature of the PRZ for both 1 mm and 2 mm high-speed jet holes. All the cases presented in Fig. 7 can be termed as stable-no ash fusion cases (H1-H8, F1, S1, P1). Varying the high-speed jet flow rates have a little influence on the PRZ temperatures. Increase in high-speed jets flow rate probably causes

opposing effects of enhanced reactant dilution reducing the temperature, and increased temperature due to increased airflow rate leading to more or less the same PRZ temperature.

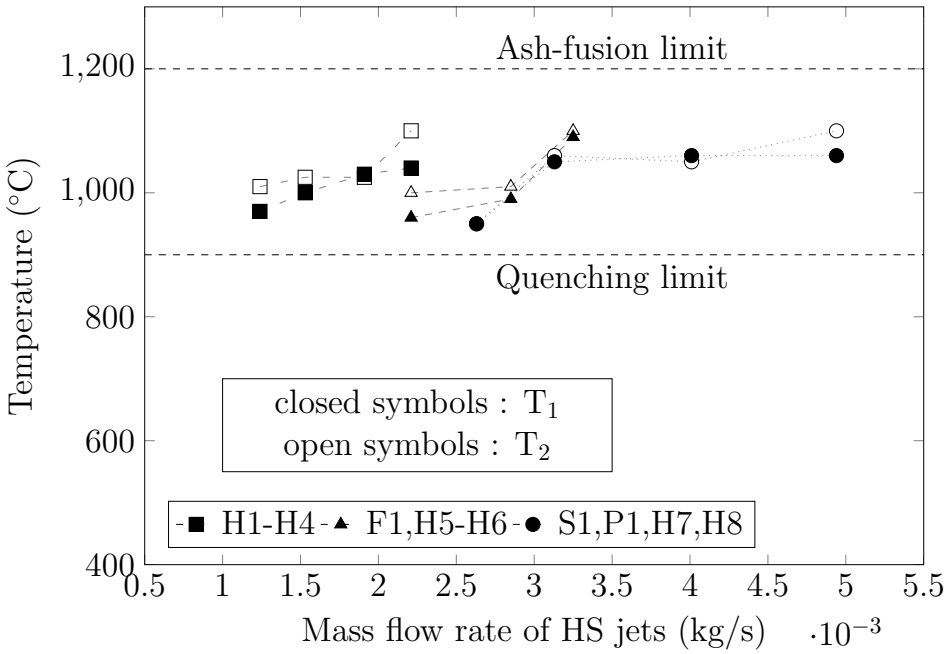

Figure 7: Temperatures in the PRZ as a function of high-speed jet mass flow rate.

3.5 Effect of particle size distribution and feed rate of coal

Two particle size distributions presented in Fig. 3 are compared for their effects on temperatures in the PRZ. The results obtained with the two distributions as a function of feed rate are shown in Fig. 8. The coarse PSD with feed rate lower than 2.08×10^{-3} kg/s (F2) leads to a quenching operating condition. However, the fine PSD is stable even with a coal feed rate of 1.11×10^{-3} kg/s. The temperatures with the fine PSD are higher than that with coarse PSD as expected.

Figure 8 also clearly shows that the temperatures in the PRZ with the fine PSD exceed the ash fusion temperature and can be categorized as stable-ash fusion cases (S2, F3-F5). Higher high-speed jets flow, with an increased dilution can possibly reduce the temperatures with the fine PSDs. This presents an area for further exploration on the role of high-speed jets in minimizing ash fusion issues in the reactor.

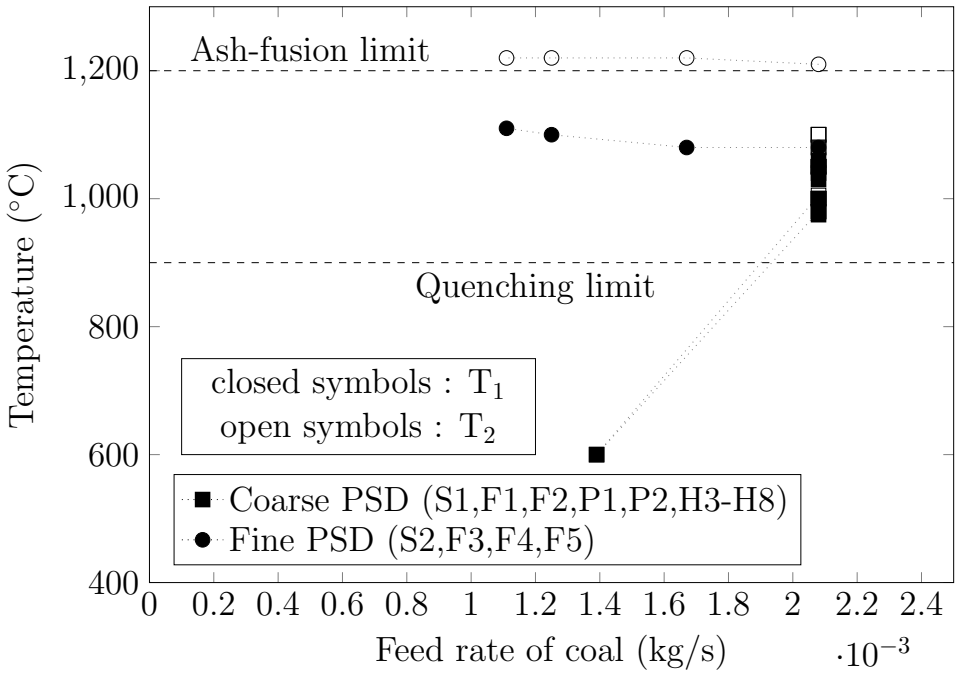

Figure 8: Effect of PSD on temperature profile in the PRZ.

The equivalence ratio (ϕ) calculated as $\frac{(A/F)_s}{(A/F)_a}$ for cases presented in Fig. 8 ranges from 1.38 – 2.92. Temperature in the reactor is insensitive to the changes in equivalence ratio, whereas it is affected by the feed rate and PSD.

In the following sections details of particle tracks, thermo-chemical conversion of particles and their relation to reactor stability are presented.

4 Particle sub-models: tracks and thermo-chemical conversion

Relative magnitudes of particle flow time (t_f) and particle ignition time (t_{ig}) are hypothesized to govern the stability of coal-air flames stabilized by high-speed jets. The following section describes the procedure and methodology for estimating particle flow times and particle ignition times.

4.1 Flow field resolution

Particle flow time requires resolution of the velocity field in the combustor. The velocity profiles of the high-speed jets stabilized recirculating flows

were numerically calculated using CFD (details are given in Appendix A). Increased velocities experienced by the coal particles due to combustion are addressed by simulating flow field with heated jets of primary and high-speed jets, and employing the velocity profiles for the calculation of particle flow time. Figure 9 presents the calculated axial centerline velocities for a few cases presented in Table 4. The centerline velocities of all the cases considered in the current work show a similar trend. Reversed flow velocities can be observed in the first half of the PRZ due to the primary jet deflection towards the high-speed jets, and velocities greater than the inlet primary jet velocity due to transfer of momentum from the high-speed jets in the second half of the PRZ. Details of the computational domain, models used and boundary conditions are presented in Appendix A.

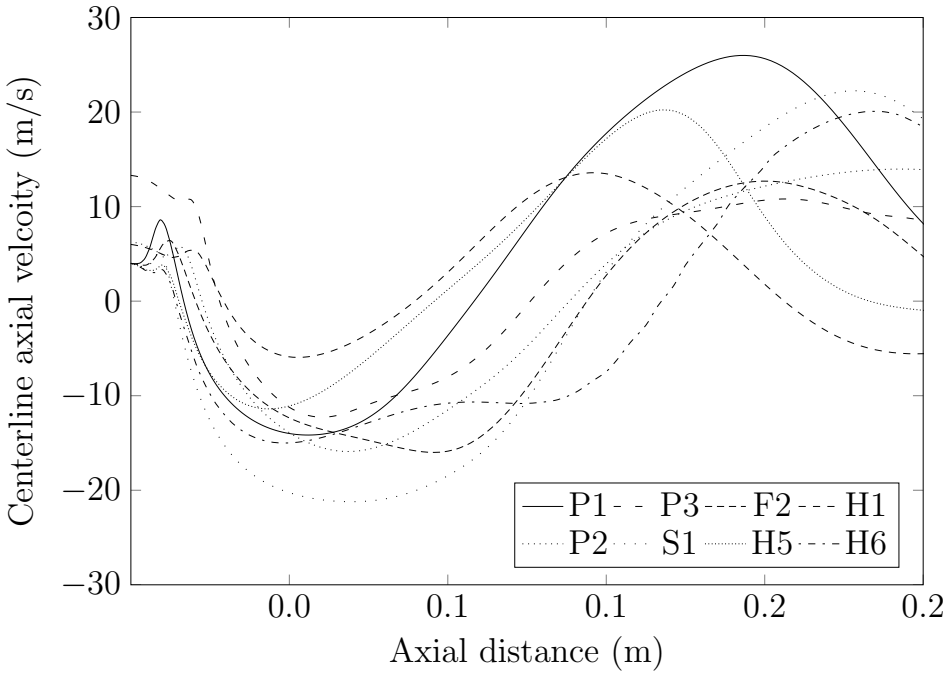

Figure 9: Calculated axial velocity profiles on the centerline of the combustor for different operating conditions.

4.2 Particle tracks and particle flow time

Particles are tracked to estimate the flow time by calculating the drag exerted by the flow-field. Flow field modification by the particles is assumed to be minimal and is not considered as the volume loading of the particles

in the primary jet itself is <1%. Therefore, the flow field is decoupled from the particle tracks. Though the particles move in all three directions, only axial displacement of the particles is considered for evaluating the particle flow time. The distance traveled by particles in the lateral direction (∼0.05 m) is smaller compared to that in the axial dimension (∼1 m). Therefore, the lateral displacement of particles is neglected in calculating the particle flow time.

Particles are tracked along the centerline of the reactor employing Equations 1–3. The deviation in particle flow time, corresponding to different initial locations of particles across the primary jet, is within ±10%. Hence, the tracking of the particles along the centerline is a reasonably good assumption for obtaining the particle flow time.

Numerically obtained centerline axial velocity (u) as shown in Fig. 9 is fit by piecewise linear functions to compute the particle velocity and position by Eqs. 2 and 3. The drag on the particle by the flow field is given by Eq. 1. Axial displacement of a particle (Δx) is estimated by integrating Eq. 1 twice accounting for time-dependent variation of particle velocity (Eq. 2) for a time interval Δt. Gas-phase velocity is updated after each time step based on the axial location of the particle. Recirculating particles are identified as those which exhibit a reversal in the direction of motion.

$$\frac{du_p}{dt} = C_d(u - u_p) \tag{1}$$

$$u_{p_2} = u - (u - u_{p_1})exp(-C_d\Delta t) \tag{2}$$

$$x_2 = x_1 + u\Delta t + \left(\frac{u - u_{p_1}}{C_d}\right) exp(-C_d\Delta t) - \left(\frac{u - u_{p_1}}{C_d}\right) \tag{3}$$

where C_d is the drag coefficient, estimated by $C_d = 18\mu/(\rho_p d_p^2)$, and u is the centerline velocity of the gases at location x, u_p is the particle velocity, and Δt is the time step for integration.

The particle flow time (t_f) is defined as the time taken by the particle to travel through the PRZ and reach the axial location of 0.2 m. The particle flow time is calculated by Eq. 3 iteratively until the axial displacement of the particle is 0.2 m or till the particle exhibits direction reversal. A flow chart outlining the procedure of calculation of flow time is presented in Fig. 10.

All recirculating particles are assumed to contribute to enthalpy addition in the PRZ. Particles for which the t_f is indicated as r in Fig. 11 are the

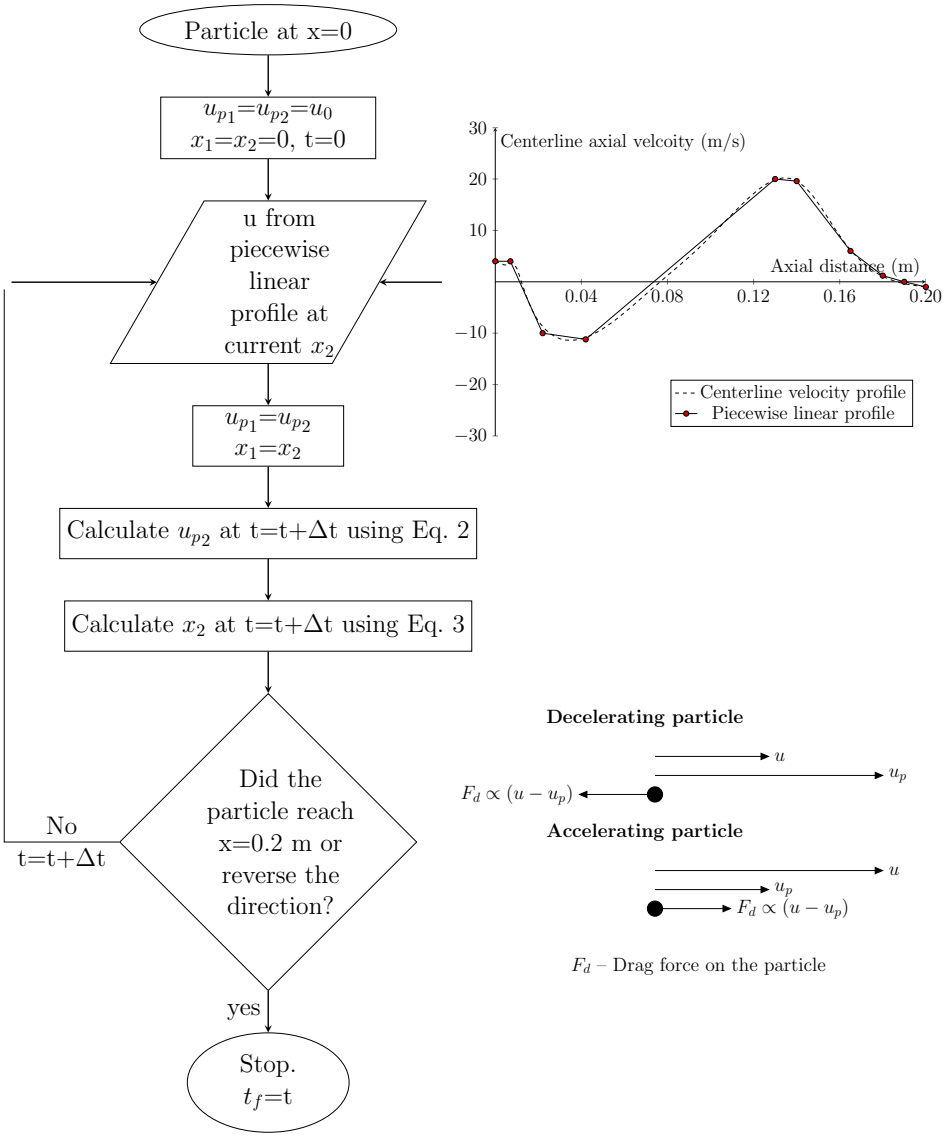

Figure 10: Flow chart outlining the procedure of t_f calculation.

ones which are recirculating. For these cases the estimated flow time is essentially ∞, indicating re-circulation. Broad behaviour of t_f for particles of different diameters is presented in Fig. 11 for H8 and P3 cases. It can be observed that t_f for particles > 82.5 μm is almost the same due to larger Stokes number of the particles.

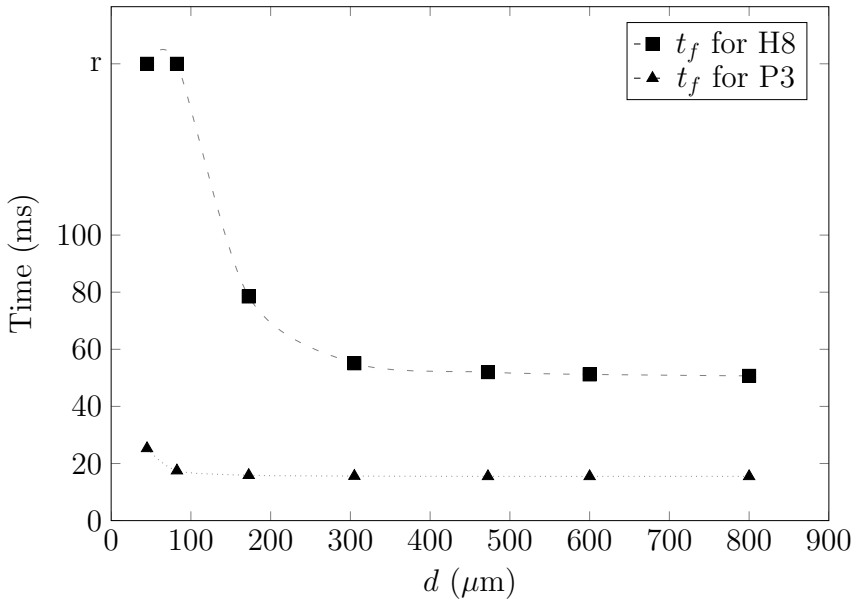

Figure 11: Flow time for different particle sizes; r on the vertical axis indicates recirculation.

Table 5 presents t_f obtained by Eq. 3 for various combinations of primary and high-speed jets flow rates. It is observed that for particle sizes >82.5 μm, there is a negligible effect of the high-speed jet momentum on t_f for high-speed to primary momentum ratios lower than 100.

Table 5: Particle flow time t_f for different operating conditions.

Expt.Name	**Particle flow time (ms)**							**Momentum ratio**
d (μm) $\rightarrow$	45	82.5	172.5	305	472.5	600	800	(High-speed/primary)
P1	r*	r	52	50.6	50.2	50.2	50.1	86
P2	r	r	37.9	34.6	33.9	33.7	33.6	66
P3	25.3	17.5	15.9	15.6	15.5	15.5	15.5	17
S1	r	r	58.5	52.3	50.9	50.6	50.41	45
S2	r	r	58.5	52.3	50.9	50.6	50.41	45
F1	r	r	68.2	54.1	51.6	51	50.6	61
F2	r	r	68.2	54.1	51.6	51	50.6	61
F3	r	r	58.5	52.3	50.9	50.6	50.41	45
F4	r	r	58.5	52.3	50.9	50.6	50.41	45
F5	r	r	58.5	52.3	50.9	50.6	50.41	45
H1	r	39.6	34.7	33.8	33.6	33.5	33.4	25
H2	r	r	37.7	34.6	33.9	33.7	33.6	21
H3	r	56.6	36.5	34.3	33.8	33.6	33.5	17
H4	r	51.4	36.1	34.2	33.7	33.6	33.5	14
H5	r	r	53.4	51	50.4	50.3	50.2	79
H6	r	r	85.4	55.7	52.1	51.3	50.7	90
H7	r	r	76.2	54.8	51.9	51.1	50.7	110
H8	r	r	78.5	55.1	52	51.2	50.7	136
H9	r	71.3	54	51.3	50.6	50.4	50.2	42

* - recirculating particle

4.3 The unified ignition-devolatilization model and particle ignition time

Results of extensive studies on different types of coals to elucidate the intrinsic kinetic behaviour (mostly using TGA-DTA and similar analytical techniques) when subject to heating can be found in the literature (see for instance Hurt et al. (1998); Sadhukhan et al. (2011); Solomon et al. (1988); Xi et al. (2020)). But it is not adequately recognized that the particles, single as well as under reactor conditions, are subject to much higher heating rates compared to that in TGA-DTA class of experiments. This difference implies that the conversion is transport controlled in realistic systems and is not limited by intrinsic kinetics. This important aspect has been clearly demonstrated for single-particles and packed bed biomass conversion (see Varunkumar et al. (2011, 2013)). The computational results of Goshayeshi and Sutherland (2014) for coal with chemical percolation devolatilization model and detailed kinetics for gas-phase and condensed phase, also show a d^2 variation with time, indicating that transport processes govern the ignition and devolatilization. Based on the above considerations, the unified ignition-devolatilization model (UID) by Jaganathan et al. (2017) is extended to study coal conversion. The model is validated against the ignition

data of Shaddix and Molina (2009) and Goshayeshi and Sutherland (2014). The deviation of the ignition times from experimental results is <10% (refer Appendix A). Most of the experimental ignition and devolatilization times for single particles in the literature could not be predicted due to the unspecified boundary conditions and properties of coal, which are required for predictions by the model.

The model estimates the mass flux of volatiles (G_p) by tracking the propagation of the pyrolysis front (r_p) into the virgin particle. The pyrolysis front is identified by the pyrolysis temperature (T_p, 400°C for coal used in the current work). The pyrolysis front separates the devolatilized and virgin regions of the particle. The temperature profile in the core is governed by unsteady heat conduction. The devolatilized zone is assumed to be quasi-steady due to the slower rate of regression of r_p compared to to the gas-phase velocity. The rate of devolatilization can be calculated by Eqs. (4) to (6). More details about the UID model can be found in the references Jaganathan (2019); Jaganathan et al. (2017).

$$\frac{G_p C_p {r_p}^2}{{r_s}^2}\left[T_s - T_p + \frac{H_d}{C_p} + \frac{c}{G_p C_p}\right] = h(T_\infty - T_s) \tag{4}$$

$$ln\left[\frac{T_s - T_p + H_d/C_p + c/(G_p C_p)}{H_d/C_p + c/(G_p C_p)}\right] = \frac{G_p C_p {r_p}^2}{k}\left[\frac{1}{r_p} - \frac{1}{r_s}\right] \tag{5}$$

$$\frac{dr_p}{dt} = \frac{-G_p}{\rho_p} \tag{6}$$

where, h is the heat transfer coefficient, T_∞ is the ambient temperature, H_d is the heat of devolatilization, C_p, and k are the specific heat and thermal conductivity of the gas-phase respectively.

Particle ignition time (t_{ig}) encompasses the effects of particle size distribution (PSD), coal feed rate and the requirement of minimum power. The minimum heat release rate required to keep the reactor from quenching was obtained by conducting a series of experiments with LPG. A stable operating condition was attained with 5 lpm LPG, 100 lpm primary flow rate, and 92 lpm high-speed jets flow rate with 1 mm holes. The reactor was quenched by maintaining the same fuel-air ratio with 3 lpm LPG. Reactor quenching at the same fuel-air ratio is a result of heat loss from the reactor. LPG flow rate of 3 lpm corresponds to a power of 5 kW.

Obtaining t_{ig} involves the identification of a representative particle size

which comprises the effects of feed rate, PSD and minimum power. The representative particle size denotes the smallest particle that is to be devolatilized to maintain the PRZ stable. The case of coarse distribution with a coal feed rate of 2.03×10^{-3} kg/s is used to outline the procedure for obtaining t_{ig}. Necessary details are presented in Table 6. The minimum power requirement of 5 kW corresponds approximately to 0.28×10^{-3} kg/s of coal feed rate assuming enthalpy addition only by the volatiles. This corresponds to a mass fraction of 13% of the total coal loading. Cumulative mass fraction of particles in size range of 150-250 μm exceed the desired fraction of 13%, and hence a mean diameter of the range (172.5 μm) is used to calculate t_{ig}.

Table 6: Computed values of t_{ig} from the heat flux limited devolatilization model.

Size range (μm)	**Mean size** (μm)	**Cumulative mass distribution** (%)	t_{ig} (ms)
< 45	45	1.4	3
45-150	82.5	7.4	14.7
150-250	172.5	15.1	59.7
250-355	305	38.1	222.8
355-500	427.5	87.3	333.8
500-700	600	99	749
> 700	800	100	1460

The particle ignition time (t_{ig}) is calculated by the UID model with a free stream temperature determined by the average of T_1 and T_2. The slip velocity between the particles and ambient gas was neglected. This introduced an error less than 1%.

5 Stability Analysis

5.1 Ignition index

In high-speed jets stabilized coal-air flames, the recirculation zone caused by the entrainment of the primary jet into the high-speed jets dominates the flow field in the reactor. The flow field inside the reactor is highly turbulent with Reynolds (Re) number based on the exit nozzle diameter of the high-speed being 18055 ($Re = ud/\nu = \frac{250\times1.3\times10^{-3}}{18\times10^{-6}}$), and based on

primary diameter it is $\sim$ 4500. Estimate of Reynolds number based on the reactor dimension ($\sim$ 6000) also suggest a highly turbulent regime. In this highly turbulent flow field, particles with a low Stokes number follow the flow into the high-speed jets, whereas, those with a large Stokes number travel straight out of the primary jet. During their travel in the reactor, particles are heated, ignited and devolatilized. The released volatiles oxidize and feed energy to the downstream endothermic processes.

A stable oxidation zone is established when the particle ignition times (t_{ig}) are shorter or of similar magnitude as that of particle flow times (t_f). Moreover, the heat release from the volatile oxidation should at least balance the heat loss from the reactor for a self-sustained flame. A non-dimensional ignition index (τ) that accounts for both these criteria is used to assess the stability of recirculating coal-air flames in the current work. The ignition index is defined as a ratio of particle flow time to particle ignition time ($\tau = t_f/t_{ig}$). Particle ignition times being shorter or of similar magnitudes as that of particle flow times implies that τ is at least of the $\mathcal{O}(1)$ for stable cases. The effects of various operating conditions are absorbed into a single parameter that describes the stability of the reactor. While the primary and high-speed jets momentum effects are accounted for by t_f, t_{ig} includes the effects of particle size distribution, feed rate and the requirement of minimum power. The stability of the oxidation zone is ascertained by temperature measurements of the primary reaction zone (PRZ).

Calculation of τ for case H8 is presented here. The representative particle diameter, as brought out earlier, based on the minimum power requirement for stability is 172.5 μm. The t_f corresponding to this diameter is 78.5 ms and t_{ig} is 59.7 ms, yielding a τ of 1.3. To calculate the ignition index of the operating conditions where the flow time of recirculating particles are involved, t_f is estimated by the smallest diameter particle that does not enter the recirculation zone. Particle ignition time (t_{ig}) for such cases, is still estimated by the minimum power criterion.

Although particles are subjected to varying heat flux and three-dimensional motion during their travel, t_{ig} and t_f calculated by the particle sub-models are taken to be representative times of the reactor conditions. The analysis presented in this paper presents a qualitative behaviour (same order of magnitude) of the stability of the reactor. Accurate quantitative estimates of τ can be calculated from a computational framework where the particle

tracks are computed with the UID model simultaneously. Computations of the same are in progress. Also, a computational framework required for capturing gasification dynamics accounting for volatile release rate by the UID model and reduction reactions of char with kinetic data is currently under development.

5.2 The stability map

Figure 12 presents all the experimental data set out onto a T-τ plot as a stability map. Temperatures measured by thermocouples T_1 and T_2 are indicated in the plot. As τ increases, the stability of the reactor also increases. Vertical dotted lines indicate the stable and unstable limits of τ accounting for the uncertainties. Operating conditions with $\tau > 0.82$ are very stable, and those with $\tau < 0.58$ are highly unstable. Most of the cases with the coarse PSD have τ values between 0.58 and 0.82 and are very sensitive to fluctuations in the PSD and feed rate. The sensitivity of coarse PSD cases to stability was also confirmed from the experiments. Horizontal dotted lines present the operational limits of the reactor in terms of ash-fusion and quenching limits.

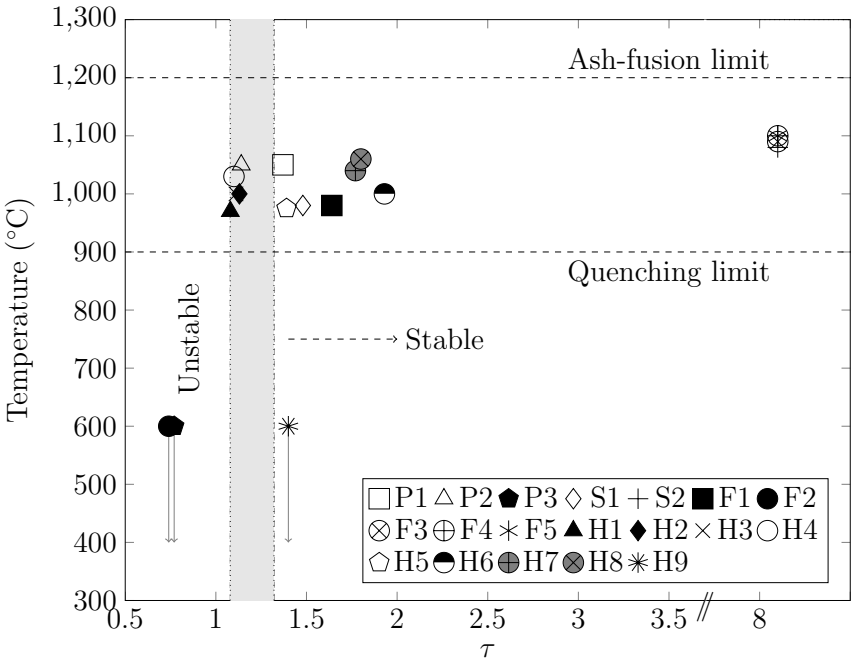

(a) T_1

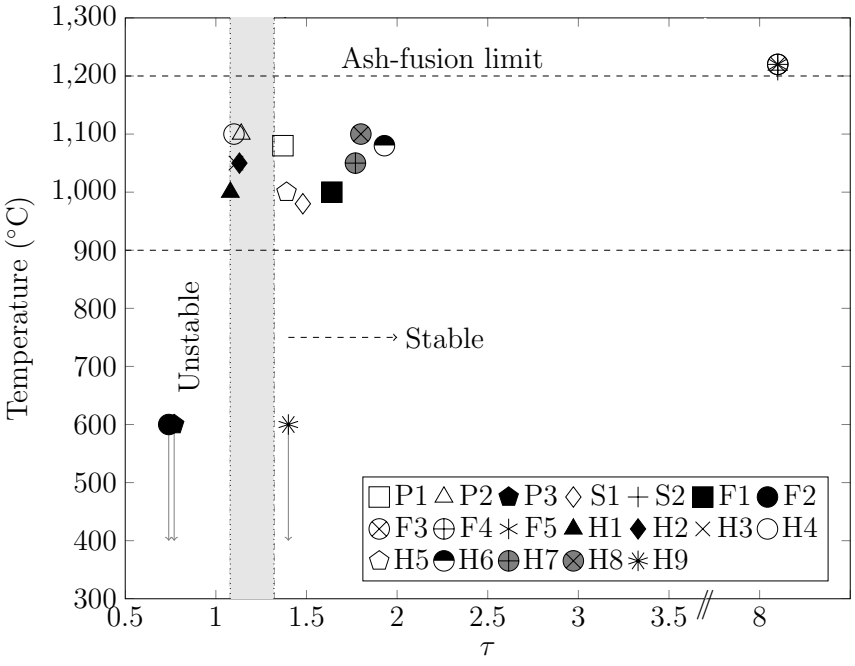

(b) T_2

Figure 12: Stability map of recirculating coal-air flames. (Note the break in x-axis after τ =3.5.)

It can be observed from Fig. 12 that as the primary velocity is increased (P1-P3), τ tends to values lower than 0.58, and leads to an unstable operating condition. An increase in the primary velocity with same PSD leads to a decrease in t_f while t_{ig} is invariant. After a critical velocity, t_{ig} exceeds t_f, leading to quenching of the reactor as can be seen with P3 ($\tau < 0.58$).

In general, the high-speed jets have minimal influence on the stability of recirculating coal-air flames (see H1-H4, F1 and H5-H6 of Fig. 12). It can be observed that the high-speed flow rate has a marginal effect on t_f for particles greater than 82.5 μm, as long as the high-speed jet to primary jet momentum ratio is less than 100 (refer Table 5). Particle flow time (t_f) is roughly the same even with an increase in high-speed jets flow rate, leading to almost similar τ values. For the cases with high-speed jets to primary jet momentum ratio >100, flow time for the representative 172.5 μm particle is higher compared to the cases with high-speed jets to primary jet momentum ratio <100. This leads to an increase in t_f, thereby enhancing τ.

The effect of PSD can be observed from the τ values of S1 and S2 operating conditions from Fig. 12. When all the other parameters except the PSD are maintained constant, the fine PSD is highly stable ($\tau \sim 8$) when compared to a coarse PSD ($\tau \sim 1$). The smallest diameter particle that is to be devolatilized for minimum power for the coarse PSD is ~ 172 μm, and for the fine PSD, it is ~ 82 μm. Due to this, t_{ig} for the coarse PSD is around 4.5 times larger than for the fine PSD. For the same flow conditions, the fine PSD has a larger τ value indicating higher stability. The temperature profile with the fine PSD has lower fluctuations than that with the coarse PSD (refer Fig. 4b). This indicates the sensitivity of the stability of the flame to fine fractions. With coarse distribution, any deviation in the fraction of fines loaded at a given instant changes the t_{ig}, causing fluctuations in the temperature profile.

While the stability with fine fractions is high (~ 8), fines also lead to ash fusion. Fused ash restricts the availability of fixed carbon necessary for gasification reactions and is detrimental to the performance of a gasifier. On the other hand, coarse distributions are marginally stable without ash-fusion. Suppression of ash-fusion and highly-stable operating conditions can be made possible with size distributions using a combination of fine (< 75 μm) and coarse (> 200 μm) particles in a bimodal distribution, and will be explored in detail in further studies.

Figure 12 indicates that the coarse PSD is sensitive to changes in the feed rate (F1, F2). Any feed rate below 2.08×10^{-3} kg/s for the coarse PSD quenches the flame. As the feed is rate reduced, the smallest diameter required for minimum power criterion is increased for the coarse PSD. This causes an increase in t_{ig} with almost similar t_f, decreasing τ. In contrast, for the fine PSD, reducing loading has no impact on the stability as can be seen from F3, F4, and F5 cases in Fig. 12. The smallest particle size for meeting the minimum power criterion with fine PSD remains the same even with a reduction in feed rate as can be seen from Fig. 3.

5.3 Stability enhancement with coal preheating

A strategy for stabilizing distributions with a large fraction of coarse particle sizes would be preheating coal to 50-100°C below the pyrolysis temperature Mukunda and Attanoor (2018). A 50°C difference is necessary to avoid bulk devolatilization and associated flashbacks of the flame. Heat up time accounts for a major fraction of the ignition time ($\sim$ 75–80%). Preheating coal to a few degrees below the pyrolysis temperature significantly reduces the time required for ignition in the reactor. The primary jet is to be heated to the same temperature ($\sim$250°C) to ensure the particles are not cooled before being transported into the reactor.

Preheating coal is probably more effective than preheating the combustion air ($\sim$ 1200°C) for increasing the stability of the coal-air flames. It is easier to preheat coal than to preheat large quantities of combustion air. Moreover, in air preheating strategy, coal particle has to be raised from the ambient temperature to the pyrolysis temperature (ΔT $\sim$ 600°C). In the case of coal preheating, coal particle has to be heated from the preheated temperature to pyrolysis temperature, ΔT is $\sim$ 50°C. Particle ignition time (t_{ig}) is shorter for coal preheating strategy than for the air preheating case, and hence has a larger τ and greater stability.

The savings in t_{ig} with various levels of preheats for different particle diameters are presented in Table 7. It can be observed that the large particles have a more significant reduction in particle ignition times with preheat than the small particles. As t_{ig} is reduced with preheated coal, stability is enhanced considerably, especially, for size distributions with a large fraction of coarse particles. Using bimodal particle size distribution and preheating strategy, the reactor can be operated in a stable mode without ash-fusion.

Table 7: Stability enhancement with different levels of preheated coal.

Particle size (μm)	**Particle time with preheat** (ms) 100°C	200°C	300°C
45	3.4	3.0	2.4
82	13.9	12.8	10.8
172.5	56.3	51.6	42.6
305	213	197	169
427.5	319	289	233
600	710	651	542
800	1390	1286	1090

6 Conclusions

This paper presents a comprehensive investigation on high-speed jets stabilized coal-air flames with an emphasis on fuel rich regimes of relevance to gasification applications. Stability regimes and operational limits of high-ash coal-air flames are explored in the current work. The salient and novel features of the current work are as follows: (1) ash-fusion with high-ash coals is suppressed by using MILD combustion technology, (2) a non-dimensional ignition index, which is a ratio of particle flow time to particle ignition time, is identified as a single critical parameter that governs the stability of recirculating coal-air flames, (3) it is recognized that bimodal distributions with a combination of fines (< 72 μm) and coarse (> 200 μm) particles are required to enhance the stability of the upstream oxidation zone without ash-fusion required for gasification of high-ash coals, (4) preheating coal 50–100 K below the pyrolysis temperature is presented as a strategy to improve the stability of recirculating coal-air flames. The results presented in the current work can be used as a base for gasification of high-ash Indian coals.

References

Cavaliere, A. and de Joannon, M. (2004). Mild combustion. *Progress in Energy and Combustion science*, 30(4):329–366.

Edland, R., Normann, F., Allgurén, T., Fredriksson, C., and Andersson, K. (2019). Scaling of pulverized-fuel jet flames that apply large amounts of excess air—implications for nox formation. *Energies*, 12(14):2680.

Fu, W. B., Wei, J. B., Zhan, H. Q., Sun, W. C., Zhao, L., Chen, Y. L., Han, H. Q., Huang, W. S., and Wu, C. K. (1988). The use of coflowing jets with large velocity differences for the stabilization of low grade coal flames. In *Symposium (International) on Combustion*, volume 21, pages 567–574. Elsevier.

Goshayeshi, B. and Sutherland, J. C. (2014). A comparison of various models in predicting ignition delay in single-particle coal combustion. *Combustion and flame*, 161(7):1900–1910.

Harris, D. and Patterson, J. (1995). Use of australian bituminous coals in igcc power generation technologies. *Aust. Inst. Of Energy J*, 13:22.

Hurt, R., Sun, J.-K., and Lunden, M. (1998). A kinetic model of carbon burnout in pulverized coal combustion. *Combustion and flame*, 113(1-2):181–197.

Jaganathan, V. (2019). *Syngas synthesis using gasification of biomass with O_2-CO_2 and O_2-steam mixtures*. PhD thesis. [Online; accessed 29-January-2020].

Jaganathan, V., Kalyani, A. M., and Varunkumar, S. (2017). Unified ignition–devolatilization model for fixed bed biomass gasification/combustion. *Energy Procedia*, 120:643–648.

Kong, L., Bai, J., Bai, Z., Guo, Z., and Li, W. (2014). Improvement of ash flow properties of low-rank coal for entrained flow gasifier. *Fuel*, 120:122–129.

Li, P., Wang, F., Tu, Y., Mei, Z., Zhang, J., Zheng, Y., Liu, H., Liu, Z., Mi, J., and Zheng, C. (2014). Moderate or intense low-oxygen dilution oxy-combustion characteristics of light oil and pulverized coal in a pilot-scale furnace. *Energy & Fuels*, 28(2):1524–1535.

Lowry, H. H. (1963). Chemistry of coal utilization: supplementary volume.

Mao, Z., Zhang, L., Zhu, X., Zhou, D., Liu, W., and Zheng, C. (2017). Investigation on coal moderate or intense low-oxygen dilution combustion with high-velocity jet at pilot-scale furnace. *Applied Thermal Engineering*, 111:387–396.

Mei, Z., Li, P., Wang, F., Zhang, J., and Mi, J. (2013). Influences of reactant injection velocities on moderate or intense low-oxygen dilution coal combustion. *Energy & Fuels*, 28(1):369–384.

Mishra, P. R., Sahu, R., and Chakravarty, S. (2020). Viscosity analysis of indian origin coal by using factsage at different temperatures. *Transactions of the Indian Institute of Metals*, 73(1):207–214.

Mukunda, H. and Attanoor, S. (2018). New pathways in clean combustion of biomass and coal via partial gasification. In *Coal and Biomass Gasification*, pages 455–472. Springer.

Patterson, J. and Hurst, H. (2000). Ash and slag qualities of australian bituminous coals for use in slagging gasifiers. *Fuel*, 79(13):1671–1678.

Ristic, D., Schneider, M., Schuster, A., Scheffknecht, G., and Wünning, J. (2008). Investigation of nox formation for flameless coal combustion. In *7th High Temperature Air Combustion and Gasification International Symposium, Phuket, Thailand*.

Sadhukhan, A. K., Gupta, P., and Saha, R. K. (2011). Modeling and experimental studies on single particle coal devolatilization and residual char combustion in fluidized bed. *Fuel*, 90(6):2132–2141.

Saha, M., Dally, B. B., Medwell, P. R., and Chinnici, A. (2016). Burning characteristics of victorian brown coal under mild combustion conditions. *Combustion and Flame*, 172:252–270.

Saha, M., Dally, B. B., Medwell, P. R., and Chinnici, A. (2017). Effect of particle size on the mild combustion characteristics of pulverised brown coal. *Fuel Processing Technology*, 155:74–87.

Saha, M., Dally, B. B., Medwell, P. R., and Cleary, E. M. (2014). Moderate or intense low oxygen dilution (mild) combustion characteristics of pulverized coal in a self-recuperative furnace. *Energy & Fuels*, 28(9):6046–6057.

Shaddix, C. R. and Molina, A. (2009). Particle imaging of ignition and devolatilization of pulverized coal during oxy-fuel combustion. *Proceedings of the Combustion Institute*, 32(2):2091–2098.

Sharma, A., Saikia, A., Khare, P., Dutta, D., and Baruah, B. (2014). The chemical composition of tertiary indian coal ash and its combustion behaviour–a statistical approach: Part 2. *Journal of earth system science*, 123(6):1439–1449.

Smart, J. and Morgan, D. (1994). Exploring the effects of employing different scaling criteria on swirl stabilised pulverised coal burner performance. *Combustion science and technology*, 100(1-6):331–343.

Solomon, P. R., Hamblen, D. G., Carangelo, R., Serio, M., and Deshpande, G. (1988). General model of coal devolatilization. *Energy & Fuels*, 2(4):405–422.

Stadler, H., Christ, D., Habermehl, M., Heil, P., Kellermann, A., Ohliger, A., Toporov, D., and Kneer, R. (2011). Experimental investigation of nox emissions in oxycoal combustion. *Fuel*, 90(4):1604–1611.

Stadler, H., Ristic, D., Förster, M., Schuster, A., Kneer, R., and Scheffknecht, G. (2009). Nox-emissions from flameless coal combustion in air, ar/o2 and co2/o2. *Proceedings of the Combustion Institute*, 32(2):3131–3138.

Suda, T., Takafuji, M., Hirata, T., Yoshino, M., and Sato, J. (2002). A study of combustion behavior of pulverized coal in high-temperature air. *Proceedings of the combustion Institute*, 29(1):503–509.

Varunkumar, S., Rajan, N., and Mukunda, H. (2011). Single particle and packed bed combustion in modern gasifier stoves—density effects. *Combustion Science and Technology*, 183(11):1147–1163.

Varunkumar, S., Rajan, N., and Mukunda, H. (2013). Universal flame propagation behavior in packed bed of biomass. *Combustion Science and Technology*, 185(8):1241–1260.

Wang, P. and Massoudi, M. (2013). Slag behavior in gasifiers. part i: Influence of coal properties and gasification conditions. *Energies*, 6(2):784–806.

Weber, R. and Breussin, F. (1998). Scaling properties of swirling pulverized coal flames: From 180 kw to 50 mw thermal input. In *Symposium (International) on Combustion*, volume 27, pages 2957–2964. Elsevier.

Weber, R., Smart, J. P., and vd Kamp, W. (2005). On the (mild) combustion of gaseous, liquid, and solid fuels in high temperature preheated air. *Proceedings of the Combustion Institute*, 30(2):2623–2629.

Weidmann, M., Honoré, D., Verbaere, V., Boutin, G., Grathwohl, S., Godard, G., Gobin, C., Kneer, R., and Scheffknecht, G. (2016). Experimental characterization of pulverized coal mild flameless combustion from detailed measurements in a pilot-scale facility. *Combustion and Flame*, 168:365–377.

Weidmann, M., Verbaere, V., Boutin, G., Honoré, D., Grathwohl, S., Goddard, G., Gobin, C., Dieter, H., Kneer, R., and Scheffknecht, G. (2015). Detailed investigation of flameless oxidation of pulverized coal at pilot-scale (230 kwth). *Applied Thermal Engineering*, 74:96–101.

Xi, Z., Wang, X., Li, M., and Wang, X. (2020). Characteristic analysis of pulverized coal combustion. *Combustion Science and Technology*, pages 1–18.

Zhang, H., Cui, K., Zhang, Y., Liu, Q., Lu, J., and Yue, G. (2017). Ignition improvement and nox reduction with local oxygen-enriched coal-fired burner. In *11th Asia-Pacific Conference on Combustion, The University of Sydney, NSW Australia*.

Zhang, H., Yue, G., Lu, J., Jia, Z., Mao, J., Fujimori, T., Suko, T., and Kiga, T. (2007). Development of high temperature air combustion technology in pulverized fossil fuel fired boilers. *Proceedings of the Combustion Institute*, 31(2):2779–2785.

A Appendix

A.1 Validation of the model

An analysis of the computational ignition data of Goshayeshi and Sutherland (2014) is done in the current study. When the ignition time data is plotted as a function of d^2, it is seen that particle ignition varies linearly with d^2 indicating that the process is transport controlled (see Fig. 13).

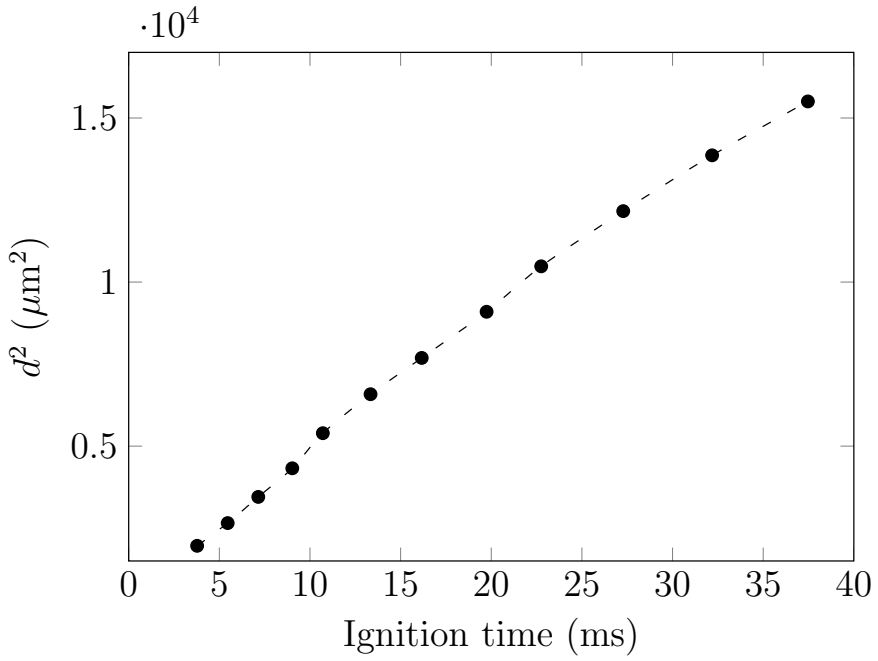

Figure 13: Data from Goshayeshi and Sutherland (2014) showing a d^2 vs t variation.

The extended UID model for coal is validated against the experimental ignition data of Shaddix and Molina (2009) and Goshayeshi and Sutherland (2014). The data used for validation from the work of Shaddix and Molina (2009) and Goshayeshi and Sutherland (2014) correspond to coal particles with a volatile fraction of 40 and 35% respectively. The furnace temperatures for the ignition experiments from their studies correspond to 1750 K and 1320 K respectively. The ignition times are estimated with an assumed pyrolysis temperature of 400°C, arrived at by mass loss analysis at 200, 300 and 400°C for coal used in current work. The change in ignition time is about 0.42 ms/°C for the choice of pyrolysis temperature for 800 μm particle diameter. The comparison of the model predictions with the experimental data is presented in Fig. 14.

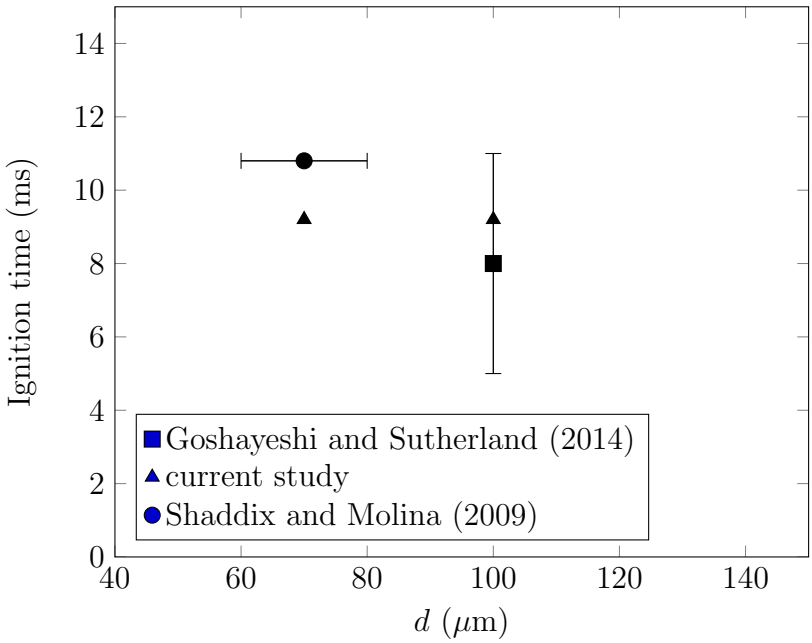

Figure 14: Validation of the UID model with data from Goshayeshi and Sutherland (2014) and Shaddix and Molina (2009).

A.2 Computational domain, models and boundary conditions

In an enclosed reactor, the high-speed jets entrain the primary jet due to a large velocity differential. A recirculation bubble is created by the entrainment of the primary jet into the high-speed jets. The recirculation zone is three dimensional, and hence a 3D model of the reactor was simulated to determine the flow field.

The first step in simulating the flow field is to identify if the flow is laminar or turbulent. Reynolds number (Re=vd/ν) based on the dimensions of the primary jet ($Re_p \sim 4500$) and the high-speed jets ($Re_{HS} \sim 18000$) show that the net behaviour of the flow field in the reactor is turbulent. Hence, a turbulent calculation is set up to resolve the flow field.

The computational domain created for the reactor is shown in Fig. 15. ICEM CFD was used to create a structured mesh to compute the flow field. Centerline axial velocity profiles were independent of the number of nodes beyond 1 million nodes. Therefore, 1 million grid points were used to compute the velocity fields in ANSYS Fluent. Velocity inlet for primary and

LPG inlets, pressure inlet for high-speed jets, zero gauge pressure for the outlet, no-slip and impermeable boundary conditions for all walls were specified. The walls were maintained at adiabatic conditions.

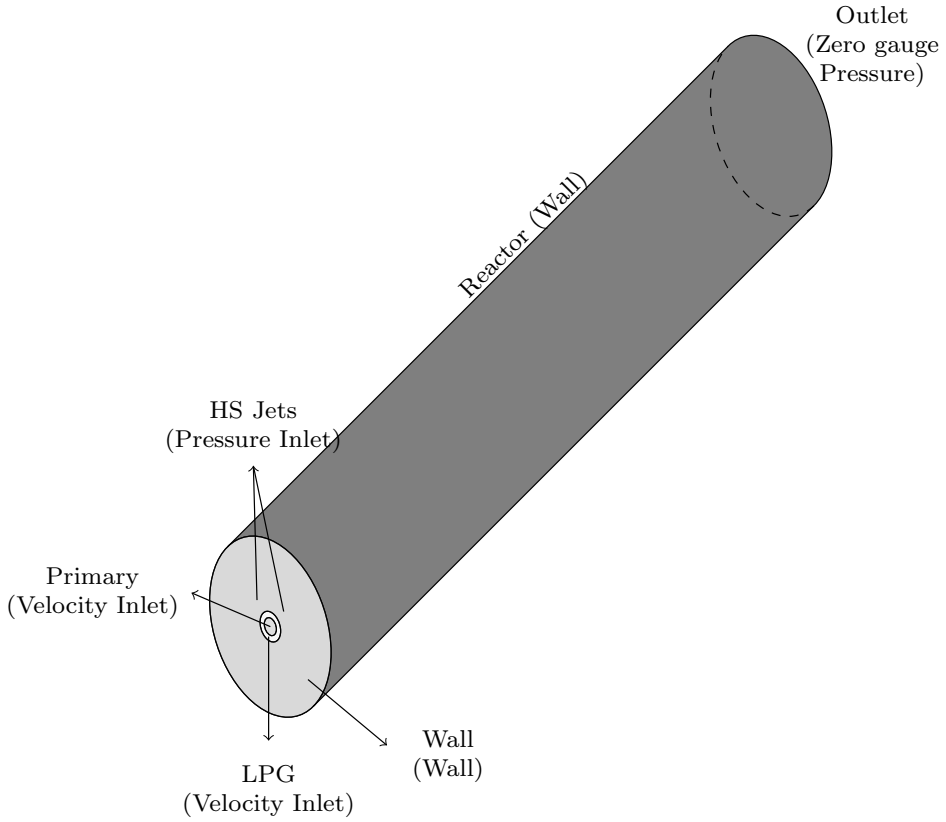

Figure 15: Computational domain and boundary conditions for the reactor.

Pressure based solver with steady formulation was used to simulate the flow field. SST k-ω model was employed to resolve the turbulence characteristics.